Available online at www.sciencedirect.com
SCIENCE DIRECT
Polymer 46 (2005) 6411–6428
polymer
www.elsevier.com/locate/polymer

The structure of crystallisable copolymers of L-lactide, ε-caprolactone and glycolide

Wasinee Channuan[a,b], Jintana Siripitayananon[a,b], Robert Molloy[b], Montira Sriyai[b], Fred J. Davis[a], Geoffrey R. Mitchell[a,*]

[a]*Polymer Science Centre, University of Reading, Reading RG6 6AF, UK*
[b]*Department of Chemistry, Chiang Mai University, Chiang Mai 50200, Thailand*

Received 11 December 2004; received in revised form 29 March 2005; accepted 1 April 2005
Available online 22 June 2005

Abstract

We apply a new X-ray scattering approach to the study of melt-spun filaments of tri-block and random terpolymers prepared from lactide, caprolactone and glycolide. Both terpolymers contain random sequences, in both cases the overall fraction of lactide units is ~0.7 and ^{13}C and ^{1}H NMR shows the lactide sequence length to be ~9–10. A novel representation of the X-ray fibre pattern as series of spherical harmonic functions considerably facilitates the comparison of the scattering from the minority crystalline phase with hot drawn fibres prepared from the poly(L-lactide) homopolymer. Although the fibres exhibit rather disordered structures we show that the crystal structure is equivalent to that displayed by poly(L-lactide) for both the block and random terpolymers. There are variations in the development of a two-phase structure which reflect the differences in the chain architectures. There is evidence that the random terpolymer includes non-lactide units in to the crystal interfaces to achieve a well defined two-phase structure.

Keywords: X-ray scattering; Structure; Orientation

1. Introduction

Copolymers of L-lactide with units such as ε-caprolactone and glycolide have been proposed and used in a wide variety of biomedical applications including absorbable monofilaments sutures [1], controlled drug release [2–4] and bone fixation [5–8]. The properties can be tailored to particular applications by adjusting the chemical configuration of the polymers in terms of the monomers used and their composition together with the thermal and mechanical treatments employed during the processing of the products. In many circumstances, the key to the definition of the properties is the control of the crystallisation of the lactide units within the copolymer structure. Homopolymers of L-lactide exhibit a number of crystalline phases whose structures have been determined from X-ray patterns of highly aligned fibres. The particular phase displayed appears to depend on the processing route of the fibres, the most common structure is the α phase which exhibits a −10/3 helical chain conformation [9–11] but hot fibre drawing may lead to the formation of the β phase which is based on a 3/1 helix [12]. As with many helical structures, interactions between neighbouring chains play an important part in stabilising particular structures and detailed work by Puiggali et al. has identified specific frustrated packing schemes which arise from differing parallel and antiparallel arrangements of neighbouring chains [12,13]. Random copolymers which contain 70 mol% or more of lactide and equivalent sequence lengths in block copolymers may exhibit some crystallinity. Clearly the local chain environment in a random copolymer may differ greatly from that in a homopolymer system. This contribution focuses on determining the structural characteristics of the crystalline component of such copolymers. These are complex materials with a number of components and phases. Analysis of the X-ray diffraction data is not all straightforward even from highly aligned fibres and we have

* Corresponding author. Tel.: +44 118 378 8573; fax: +44 118 975 0203.
E-mail address: g.r.mitchell@reading.ac.uk (G.R. Mitchell).

0032-3861/$ - see front matter © 2005 Published by Elsevier Ltd.
doi:10.1016/j.polymer.2005.04.097

developed a new approach which facilitates the comparison of data from partially oriented, poorly ordered systems. In particular we contrast a random terpolymer and a tri-block terpolymer with similar overall compositions but with different distributions of monomer units within the polymer chain and explore if the 10/3 helical chain conformation of crystalline poly(L-lactide) [14], is replicated in these copolymers.

2. Materials

L-lactide (LL) and glycolide (G) were synthesized using established procedures from L-lactic acid and glycolic acid (purchased from CARLO ERBA Reagenti) and purified by re-crystallization from ethyl acetate to a purity of 99.8 mol% determined by DSC. ε-Caprolactone (CL) was purchased from Aldrich Chemicals and purified by distillation under reduced pressure and stored over molecular sieves. Stannous octoate was purchased from Sigma Chemical Co. Ethyl acetate and diethylene glycol were distilled before use.

Poly(L-lactide) was synthesized by bulk polymerization of L-lactide using stannous octoate as a catalyst at 140 °C for 72 h. A random copolymer, P(LL-ran-CL-ran-G) was prepared by simultaneous addition of three monomers with a feed ratio of LL:CL:*G*=70:25:5 (mol%) into a reactor in the presence of 0.04% (w/w) stannous octoate at 140 °C for 18 h initially under a dry nitrogen atmosphere and finally under reduced pressure [15,16].

A block copolymer P(LL-ran-G)-block-P(LL-ran-CL)-block-P(LL-ran-G) (Fig. 1) was prepared using a two stage approach. First, a soft centre-block containing a random distribution of LL and CL units was prepared through melt phase polymerisation at 140 °C for 10 h with stannous octoate as a catalyst and diethylene glycol as an initiator. This 2 hydroxy-terminated (P(LL-ran-CL)diol) was used as a macro initiator for the subsequent polymerisation of the end blocks containing a random distribution of LL and G at 150 °C for 10 h [4,17]. Homopolymerization of the LL is inhibited by the consumption of the stannous octoate during the first phase. The soft centre-block was prepared using a charge of 4:5 in terms of LL and CL. The two hard end-blocks were prepared using a charge of 10:1 in term of LL and G.

In all cases the polymers were vacuum-dried at 100 °C for 24 h to remove any unreacted monomers. Typically, polymer yields of 98 w/w% were obtained.

3. Polymer characterization

The chemical compositions of the terpolymers were determined from the peak area integrations in the ^{1}H NMR spectra, the peak at $\delta=5.0$–5.3 ppm corresponding to the methine hydrogen (CH) in the LL units, at $\delta=4.0$–4.2 ppm corresponding to methylene hydrogen (CH_2) attached to the oxygen in a repeating CL unit and the area of the peak at $\delta=$ 4.5–4.9 corresponding to methylene hydrogen in the G units. Expanded sections of the proton NMR are shown in Fig. 2 and the compositions of the terpolymers obtained are shown in Table 1. The compositions largely reflect the feedstock although in the case of the lactidyl units an excess was observed in the block polymer with an observed composition of 76 mol% compared with an expected composition of 70 mol%.

Table 1 also shows the number-average molecular weight (M_n), the polydispersity index (M_w/M_n) and the intrinsic viscosity, [η] for the polymers prepared in this work. The molecular weight data for the terpolymers were determined by gel permeation chromatography (GPC) in tetrahydrofuran using polystyrene standards. The intrinsic viscosities, [η], of the poly(L-lactide) were measured with Ubbelohde viscometer in chloroform at 30 °C and used to

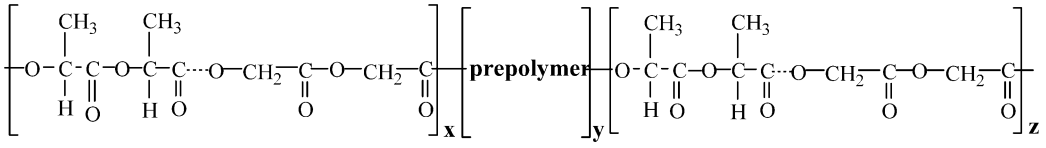

P((LL-ran-G)-b-(LL-ran-CL)-b-(LL-ran-G))

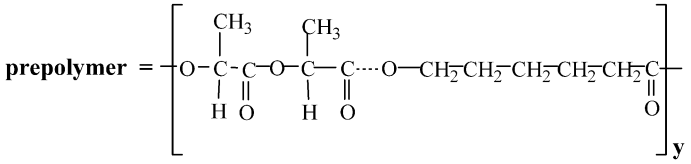

P(LL-ran-CL)

Fig. 1. A schematic of the chemical configuration of the block terpolymer used in this work showing the composition of both the prepolymer or macro initiator and the terminal blocks.

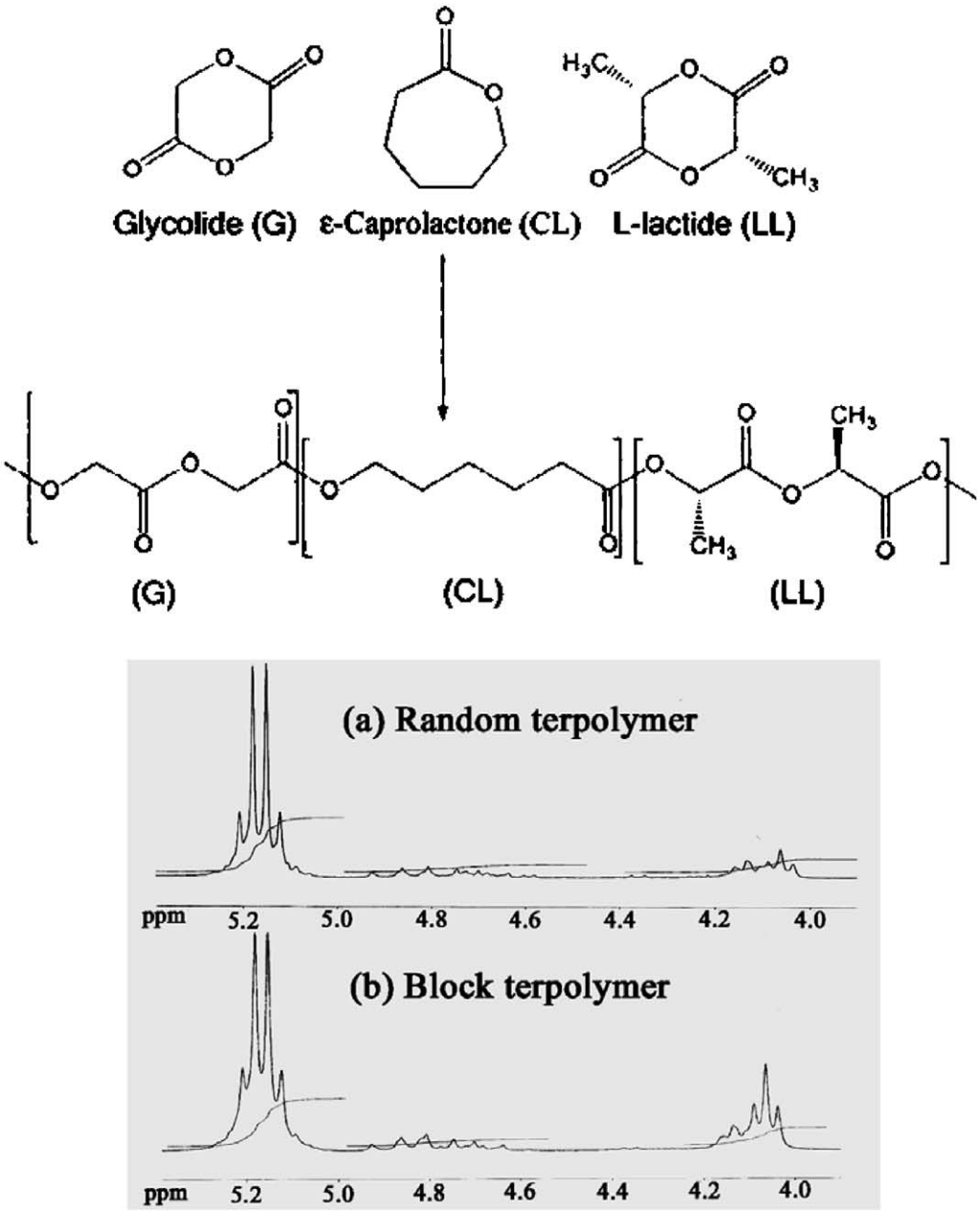

Fig. 2. A schematic of the monomers and the resultant polymer sequences and the nmr spectra used to determine the distribution of carbonyl groups in each section.

Table 1
Characterisation of polymers

Polymer	GPC		[η] (dl/g)	^{1}H NMR monomer composition LL:CL:G (mol%)
	M_n	M_w/M_n		
Poly(L-lactide)	12,000	–	0.45	–
Random terpolymer	33,000	1.85	1.27	76:19:4
Block terpolymer	27,000	1.71	0.98	71:25:4

estimate M_n using the calibration equation proposed by Nijenhuis et al. [18].

$$[\eta] = 3.25 \times 10^{-4} M_n^{0.77} \mathrm{d}Lg^{-1}$$

The properties of the materials produced, in particular the phase behaviour, are influenced by the length of sequences of individual monomer units [19–21]. In the polymers considered here, these structural characteristics can be determined by NMR. Both ^{13}C and ^{1}H NMR can be used to this end [22], The polymers under investigation are terpolymers produced by the ring-opening polymerisation of the three monomers shown in Fig. 2. Consideration of the monomers reveals that the polymerisation reaction will

inherently produce twin sequences of the lactidyl (L) and glycolidyl (G) units; with the caproyl (Cap) groups appearing as single units. However, previous studies suggest that the system will be more complex than this with transesterification producing 'unexpected' sequences such as CapLCap [23].

The assignment of individual sequences from the NMR spectra used here is based on the work of Dobrzynski [22], which is in turn based on a body of work concerning chain sequences of the various combinations of two of the three monomer units. For example, copolymers of L-lactide and ε-caprolactone have been analysed [24,25]. The analysis makes use of the carbonyl signals from the ester units; for sequences containing only caprolactone, a singlet is observed at 173.5, while for the lactate-based system the homopolymer shows a signal at 169.6 ppm.[1] The situation is made more complex for the lactidyl and glycodyl units by the fact that once the symmetry is reduced by the presence of co monomer units, the two carbonyls in the repeat unit exhibit different chemical shifts. The presence of transesterification in the polymer can be detected by the presence of isolated lactidyl or glycodiyl units [25].

The analysis uses the triad sequences to determine the average block length of the individual components as given in Eq. (1) (where X may be for example one half of the lactidyl unit and Z may be either Caprolactyl or glycidyl).[2] Where the technique is sensitive to longer sequences, and this is particularly the case for ^{13}C NMR, the triad sequences need to be calculated from (for example pentad) sequences. Thus, for example, the CapLLCap sequence contains 1 CapLL and 1 LLCap triad and must be weighted accordingly [26]. We have used both ^{13}C and ^{1}H NMR data to analyse the sequence distribution and the data obtained are shown in Table 2

$$l_{XX} = \frac{1}{2}\frac{XXX + ZXX + XXZ + ZXZ}{ZXZ + \frac{1}{2}(XXZ + ZXX)} \quad (1)$$

The sequence lengths appear to largely reflect the distributions expected for random copolymers with more or less equal reactivities. The main differences in the NMR between the so-called block and random samples is that the block terpolymer sample clearly shows a much higher proportion of the CapCapCap triad than is observed for the random sample with 60% for the block and 37% for the random. This of course is entirely in line with expectations based on the method used to synthesize the materials. In particular, since in the block copolymer the caprolactone is restricted to one of the blocks, the overall equivalent concentration appears contiguously in longer sequence lengths than broken up as in the random terpolymer. No

Table 2
Sequence lengths for copolymer system

Terpolymer	Sequence length		
	l_{LL}	l_{GG}	l_{Cap}
Block ^{1}H	8.1	0.79	3.8
Block ^{13}C	7.5	[a]	4.0
Random ^{1}H	9.0	0.85	2.3
Random ^{13}C	9.8	[a]	2.2

[a] Unable to assign peaks unambiguously hence no value available.

conclusion could be drawn from the glycidyl units from the ^{13}C NMR because of difficulties assigning the NMR peaks unambiguously, however, the data from the ^{1}H NMR is included. The only other particularly noticeable feature is that a signal which can be assigned to a CapLCap triad is observed for the block sample, but not for the random sample. It is the presence of this unit that may in part explain the lower average lactidyl sequence length for the block polymer. Apart from this peak, there is some evidence for anomalous CapLCap and GLG sequences; however, these are not a major feature of the NMR. Thus it would seem transesterification has little effect on the lactidyl units. The glycidyl units in contrast seem rather more effected by this process and a peak at 4.81 ppm in the ^{1}H NMR which can be related to the presence of isolated glycidyl units is the most prominent in this region of the spectrum. As a consequence, the average sequence length for the glycidyl units is less than 1. One final feature of the ^{1}H NMR which is worthy of note, is that while most of the spectrum is comparable to that given by Dobrzynski [22], the caprolactone region differs substantially. In particular the CapCap sequences are present in substantially higher concentrations than the GCap and LCap sequences; in the NMR presented by Dobrzynski for a polymer of similar composition, the situation is reversed. This presumably relates to the different method of polymerisation used.

In the case of the block copolymer, there are two types of lactidyl sequences. The first are those involving the copolymerisation of lactide with capraloctone to form the macro initiator or middle block and the second are those located in the end blocks copolymerised with gylcolide. It is not possible to differentiate in the NMR spectra between these two types of sequences and as a consequence the estimate of the average sequence length involves an average over the two types. If we assume that for the centre block, the units are arranged randomly according to composition alone we can estimate that the sequence length of the lactide units in the two outer blocks is ~10. As the molecular weight data were obtained from GPC measurements calibrated with polystyrene standards, there will always be some doubt as to the absolute values. However, if we combine the GPC and NMR data, we can develop a picture of the block copolymer with the middle block containing some 80–90 CL and LL units, while the end blocks each contain some 50–60 units which are largely LL. The CL

[1] The chemical shifts are quoted from the appropriate publications, these values may vary slightly with for example change of solvent; the relative positions should remain unchanged.

[2] The factor of 1/2 is only suitable for the double monomer units.

units are restricted to this central block. Within the end blocks, the LL units exhibit an average sequence length of ~10, separated by glycolide units. In contrast, the random terpolymer contains LL sequences of some 9 units but which are distributed throughout the chain separated by either glycolide units or short sequences of caprolactone. The caprolactone units are distributed throughout the chain.

4. Experimental

4.1. Wide-angle X-ray scattering

Wide-angle X-ray scattering measurements were made using a symmetrical transmission diffractometer equipped with a graphite monochromator and pinhole collimation and a Cu K-source. The intensity values from isotropic samples were obtained as a function of $|Q|$ over the range 0.2–6 Å^{-1} in steps of 0.02 Å^{-1} where $|Q| = 4\pi \sin\theta/\lambda$, 2θ is the scattering angle and λ is the incident X-ray wavelength. Data for anisotropic samples were obtained both as a function of $|Q|$ over the range 0.2–6 Å^{-1} in steps of 0.02 Å^{-1} and of α, over the range 0–90° in steps of 2°. α is the angle between the symmetry axis of the sample and the scattering vector Q. The scattering data were corrected for the effects of absorption, polarisation, multiple and incoherent scattering and scaled to absolute units using standard procedures [27]. Samples for scattering measurements were prepared by mounting lengths of fibres in a close packed parallel array. Typically the X-ray beam samples 2–3 fibres.

The rate of crystallization and the final fraction of crystallinity in each polymer were determined using a 2-circle X-ray diffractometer equipped with a graphite monochromator, pinhole collimation and a Cu-source. The diffractometer contained a heating stage for mounting 2 mm diameter Lindemann glass capillaries which allowed the temperature to be controlled within ±1 °C. Samples were melted in a Lindemann glass capillary and quenched rapidly using iced water. Subsequent X-ray scattering measurements showed these samples to be completely non-crystalline. The hot-stage used for the X-ray scattering measurements were preheated to the selected isothermal crystallisation temperature and the capillary rapidly lowered in to the hot-stage. At this stage, the wide-angle X-ray scattering data were collected to follow the nature of the crystallisation process. A series of short scans centered on $|Q| = 1.18$ Å^{-1} were taken on a continuous basis to monitor the development of a crystalline structure and the intensity recorded as a function of time. After the crystallization process was completed, the scattered intensities were recorded as a function of $|Q|$ from 0.2 to 6.0 Å^{-1} in step of $\Delta Q = 0.02$ Å^{-1}. Estimates of the crystallinity were made by separating the crystalline and non-crystalline components of the wide-angle X-ray scattering data using standard non-linear least squares peak-fitting procedures in the region $|Q|$ from 0.5 to 2.0 Å^{-1}. The fraction of crystallinity was calculated from the ratio of the $|Q|^2$ weighted integral of the crystalline peaks to the equivalent integral for the total scattering. Such an approach yields the fraction of crystallinity as a function of time, which enabled the rate of conversion or crystallisation rate to be evaluated for each particular isothermal crystallisation temperature.

4.2. Small-angle X-ray scattering

Small-angle X-ray scattering experiments were performed on the fixed wavelength ($\lambda = 1.4$ Å) beam-line 16.1 at the Daresbury synchrotron radiation source (UK) using a beam ~0.3 mm diameter. Small-angle X-ray scattering (SAXS) data in the range $|Q| \sim 0.01$–0.12 Å^{-1} were recorded using a 2-D RAPID detector with a data accumulation times of 10 s. The intensity data were normalised to the incident beam using the values obtained from an ionisation chamber prior to the sample. The SAXS detector was calibrated in terms of geometry using the scattering from a collagen sample obtained from a rat tail tendon mounted in place of the fibre samples.

4.3. Optical microscopy

The morphology of thin films of the polymers was investigated using a Swift-Bassett polarizing microscope equipped with a Mettler-Toledo programmable hot stage. The thin films were prepared by melting and pressing a small quantity of the polymer between two glass slides on a hot bar. Specimens were cooled at 20 °C/min from the melt and then, isothermally crystallized at the selected temperature.

4.4. Thermal analysis

The glass transition temperature (T_g) and the melting behaviour of the polymers were measured by differential scanning calorimetry (DSC, Perkin–Elmer 2). The instrument was calibrated with indium, dodecane and ammonium sulfate. Each sample of ~5 mg was heated at a rate of 20 °C/min in the range of −70–180 °C in all cases, except for Poly(L-lactide) for which a scan rate of 10 °C/min and a range of 20–200 °C was employed. Thermal degradation data were obtained by TGA7 thermo-gravimetric analyzer at a heat rate of 20 °C/min and heat from 50 to 600 °C under dry nitrogen.

4.5. Fibre drawing

Initial monofilaments were prepared using a small-scale melt spinning apparatus employing a batch size of 5–10 g. The processing parameters used to prepare monofilaments of the random terpolymer, the block terpolymer and poly(L-lactide) monofilaments are shown in Table 3. Using this approach monofilaments with a

Table 3
Conditions used for monofilament preparation

Polymer	Extrusion chamber temperature (°C)	Extrusion rate (mm/min)	Cooling bath (10–15 °C) used	Windup speed (mm/min)
Random terpolymer	155	0.07	Yes	0.5
Block terpolymer	167	0.10	Yes	1.0
Poly(L-lactide)	195	0.05	No	3.0

smooth surface were successfully produced with diameters of 0.4–0.6 mm. These as-spun fibres were then vacuum dried and kept in a vacuum dessicator until required.

The as-spun monofilaments were subjected to a variety of coupled mechanical and thermal treatments in order to produce samples with highly oriented crystalline structures. These conditions are shown in Table 4. The annealed samples were used for the initial structural analysis. The mechanical properties of the unannealed filaments are more typical of the requirements for absorbable monofilament sutures [2].

5. Crystallisation from a quiescent melt

The wide-angle X-ray scattering curves (Fig. 3) measured at room temperature for samples of the three polymers which have been cooled from the melt exhibit both sharp and broad peaks typical of a semi-crystalline polymer. The three patterns show considerable similarity. The data for poly(L-lactide) has substantial peaks at $|Q| \sim 1.12$, 1.28, 1.98 and 2.2 Å^{-1}. The random terpolymer sample shows peaks at $|Q| \sim 1.16$, 1.32 and 2.14 Å^{-1} while the block terpolymer samples sharp peaks at $|Q| \sim 1.14$, 1.30, and 2.14 Å^{-1}. It is not surprising that the sharp peaks in the patterns of the two terpolymers are somewhat broader and relatively less intense than the similarly positioned peaks for the poly(L-lactide).

The crystalline nature of the two terpolymers was further supported by the observation that samples cooled from the melt exhibited a strong, birefringent scattering texture, albeit with no distinctive features on scale accessible in an optical microscope. However, samples crystallised isothermally at temperatures close to the melting point revealed a distinctive banded spherulitic structure (Fig. 4) with spherulite diameters of ~70–140 μm. Poly(L-lactide) crystallised under equivalent conditions exhibited non-banded spherulites. The observation of the banded spherulites in the case of the terpolymers and not in the homopolymer serves to underline the basic precepts of the banded spherulite model proposed by Bassett et al. [28]. Optical microscopy studies during crystallisation reveal a typical linear spherulite growth rate. It was clear that the spherulite growth rate of the block copolymer is about twice that of the random terpolymer at the equivalent quench step below the melting point. The growth rate will be both a function of the composition and the sequence distribution as well as the molecular weight. As the homopolymer studied here has a different molecular weight to both block and random terpolymers, we have plotted in Fig. 5 the radial growth rates observed at a temperature corresponding to a constant degree of under cooling of $(T_m - 40)$°C for the three polymers produced in this study as a function of molecular weight along with some additional data for poly(L-lactide)s of different molecular weights taken from the literature [29–31]. The growth rates for the two terpolymers fall substantially below the fitted line for the poly(L-lactide). Clearly the chemical microstructure of the terpolymers has greatly reduced both growth rates with the random terpolymer being the most affected.

The results of the DSC studies of the three polymers are shown in Table 5. The glass transition temperature and melting point for the poly(L-lactide) are similarly to those reported in the literature, for example [31]. Equivalent DSC studies of the block and random terpolymer samples reveal somewhat lower glass transition and melting temperatures as is expected for random copolymers. We have calculated the glass transition and the melting temperature using the Fox and Flory equations [20,32] using the values of the equilibrium melting temperature and enthalpy change for the equivalent homopolymers [33,34] and these are recorded for the random terpolymer in Table 5. The correspondence between experimental and predicted values underpins the random nature of the terpolymer. Thermo gravimetric studies showed that the onset of significant degradation did not take place until ~250 °C.

In order to investigate the crystallisation behaviour of the two terpolymers in more detail, we carried out isothermal crystallisations at a series of temperatures using wide-angle X-ray scattering techniques as described earlier to evaluate

Table 4
Drawing conditions for the post-spinning treatment

Polymer	Drawing temperature (°C)	Draw rate (%/min)	Draw ratio	Annealing temperature (°C)	Annealing time (h)
Random terpolymer	40	300	4.0	–	0
Random terpolymer	40	700	8.0	80	24
Block terpolymer	40	1000	4.5	–	0
Block terpolymer	40	1000	8.0	90	1
Poly(L-lactide)	70	2400	5	90	24

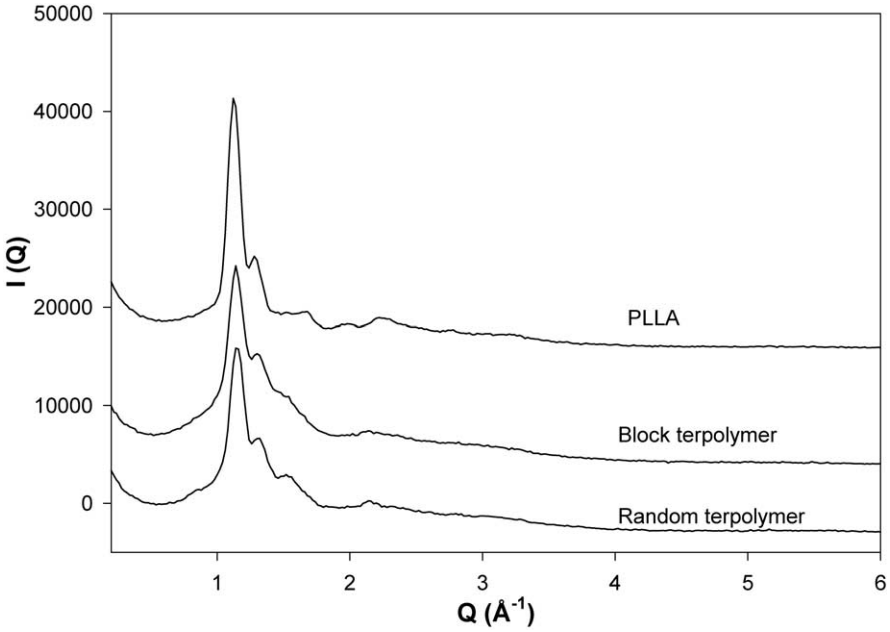

Fig. 3. Plots of the experimental wide-angle X-ray scattering intensity $I(Q)$ recorded for samples of poly(L-lactide) (PLLA), random terpolymer and block terpolymer crystallised from a quiescent melt.

the level of crystallinity. We used the intensity of the sharp diffraction feature at $|Q| \sim 1.2$ Å^{-1} recorded as a function of time to evaluate the crystallization rate or conversion rate at each temperature. Fig. 6(a) shows a plot of the rate of crystallisation for a range of isothermal crystallisation temperatures for the two terpolymers. These data reveals the typical bell-shaped curve with a maximum crystallisation rate for the random terpolymer at ~90 °C and for the block terpolymer at 100 °C. We have also plotted (Fig. 6(b)) the plateau level of crystallinity observed at the end of each crystallisation sequence. These measurements were made by separating the crystalline and non-crystalline components of the wide-angle X-ray scattering data using standard peak-fitting procedures as described earlier. Over the temperature range 50–120 °C the fraction of crystallinity lies in the range of 15–20%. There is a suggestion that the random terpolymer exhibits a slightly higher level of crystallinity at lower temperatures.

6. Structure of hot drawn fibres

6.1. Fibre patterns and related data

In order to obtain more detail on the structure of the crystalline components in the two terpolymers we have obtained maps of the X-ray scattering data for hot drawn fibres of the three polymers and these are shown in Fig. 7. Although these have the superficial appearance of traditional X-ray fibre patterns, it is emphasised that these

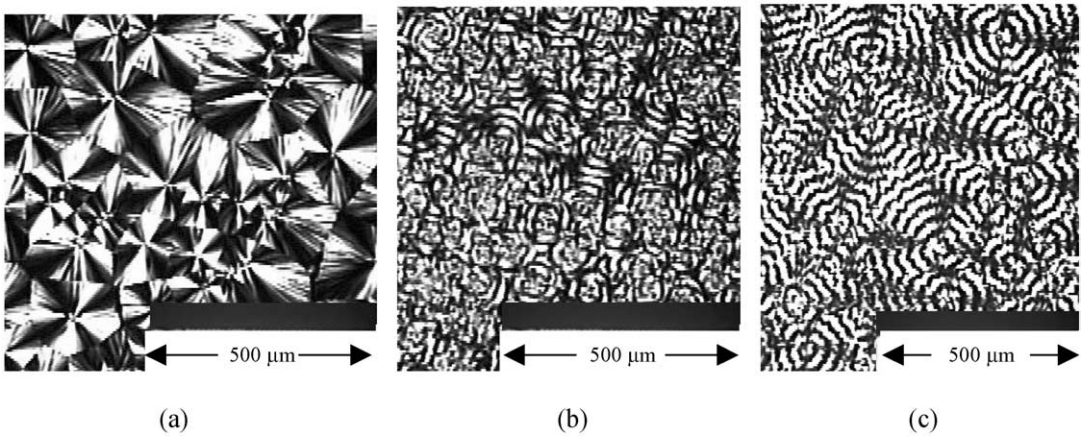

Fig. 4. Polarising optical micrographs of thin films at room temperature after crystallisation at (a) 130 °C, poly(L-lactide); (b) 110 °C random terpolymer and (c) 120 °C block terpolymer showing well defined spherulites which for (b) and (c) are strongly banded.

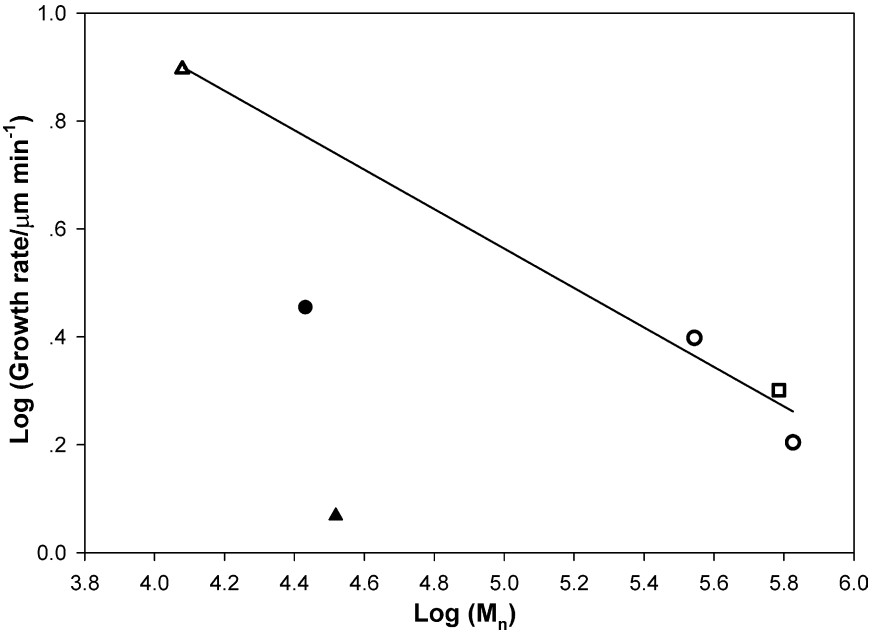

Fig. 5. A plot of the radial growth rate of spherulites against the molecular weight (M_n) for ▲ random terpolymer, ● block terpolymer and △ poly(L-lactide) prepared in this work together with data for poly(L-lactide) taken from Ref. [30] (○) and Ref. [31] (□). The growth rates were measured at a constant degree of undercooling of ~40 °C. The line represents a fit to the poly(L-lactide) data on the basis of a simple power law relationship between growth rate and molecular weight.

are true undistorted reciprocal space maps of the scattered intensity. The vertical or meridional axis is a parallel to the fibre axis and is the axis of cylindrical symmetry. The horizontal or equatorial axis lies normal to the fibre axis. The point marked 0,0 would correspond to the central part of a traditional fibre pattern. The accompanying sections show the intensity along the meridional and equatorial sections. All three fibres exhibit a high level of preferred orientation such that in all three patterns it is possible to identify the layer line structure associated with a single crystal type texture with rotational symmetry about the fibre axis. There is clearly considerable similarity between the patterns.

The poly(L-lactide) pattern has peaks in equatorial section at $|Q| \sim 1.14$, 1.46 and 1.96 Å^{-1}. On the meridional section there is a prominent peak at $|Q| \sim 2.14$ Å^{-1}. Three crystal phases have been observed for poly(L-lactide). The most common form exhibits an orthorhombic unit-cell (a= 10.7 Å, b=6.45 Å and c=27.8 Å) in which the molecules adopt a 10/3 helical conformation. Hoogsteens et al. found that by adjusting the fibre processing conditions, two other structures may be observed [10]. The so-called beta structure also exhibits an orthorhomobic unit cell (a= 10.31 Å, b=18.21 Å and c=9.00 Å) in which the molecules possess a 3/1 helical conformation [10]. The third possibility is the γ phase which is formed by the frustrated packing of three fold helices within an orthorhombic unit cell with $a=b=10.52$ Å and $c=8.8$ Å. The basic features observed in Fig. 7(a) match those reported for the alpha phase of poly(L-lactide) [10] both in terms of the position and intensity distributions of the meridional (c repeat) and the $hk0$ equatorial reflections.

In Fig. 8 we have plotted horizontal sections of the data shown in Fig. 7(a) taken at regular intervals of $2\pi/c$ corresponding to the so-called layer lines on which scattering intensity is confined for a uniaxial fibre. We observed, as expected for the α phase, that the first layer line with intensity peak on the meridian corresponds to the 10th

Table 5
DSC data

Polymer	DSC					TGA
	T_g (°C)	T_g Calc[a] (°C)	T_m[b] (°C)	T_m Calc[c] (°C)	ΔH_m (J/g)	T_d range (°C)
Poly(L-lactide)	57.8		179.3		43.6	248–378
Random terpolymer	−33.3, 34.8	35.4	143.9	143.5	7.65	252–390
Block terpolymer	41.7		156.3		25.2	254–430

[a] Calculated using the Fox equation [32].
[b] T_m is taken at the maximum of the endotherm.
[c] Calculated using the Flory equation [20] and data from Refs. [33,34].

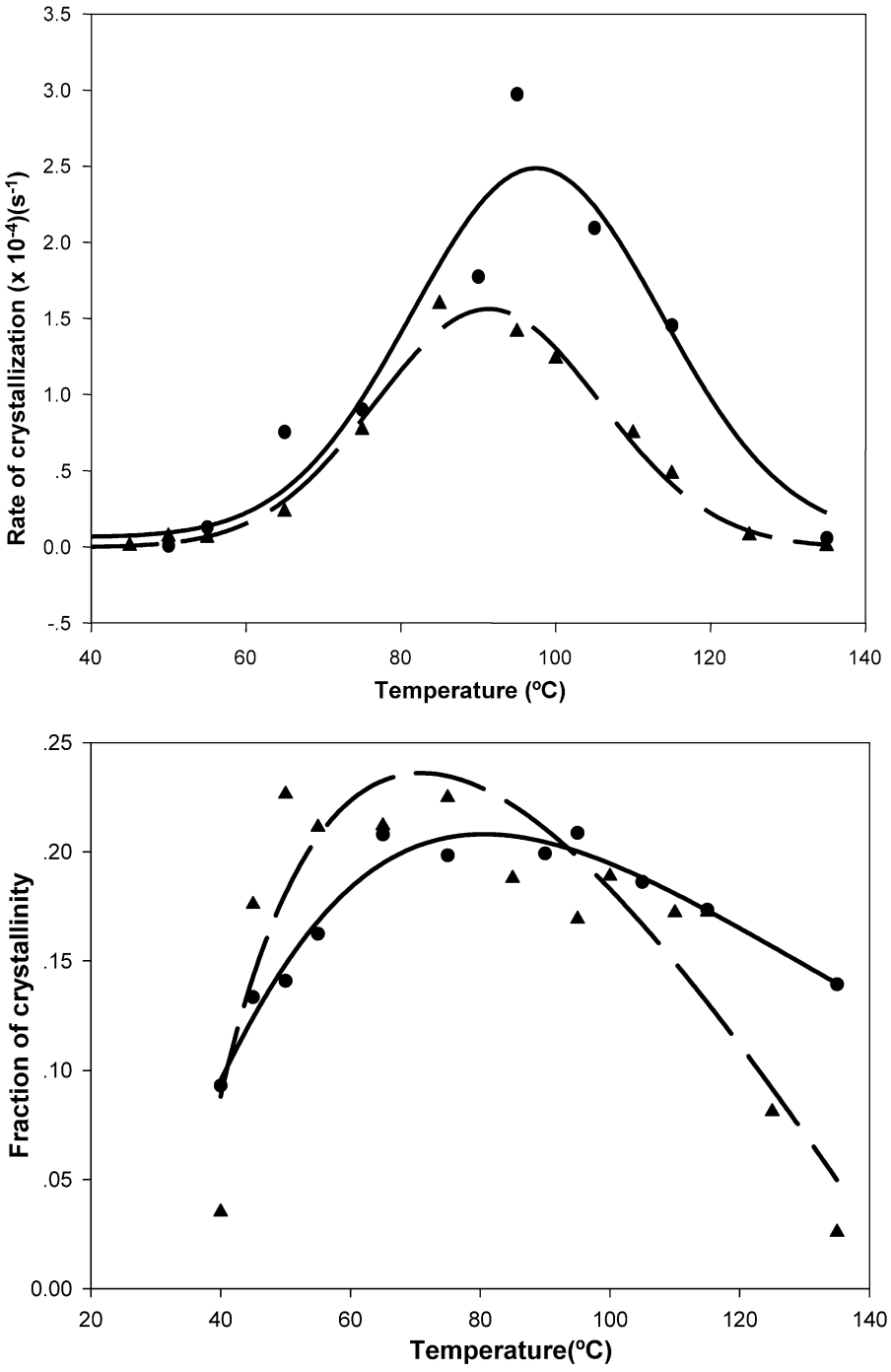

Fig. 6. (a) A plot of the rate of crystallisation as a function of the isothermal crystallisation temperature for the random terpolymer (▲, dashed-line) and the block copolymer (●, full line) derived from time-resolving wide-angle X-ray scattering data; (b) a plot of the final fraction of crystallinity in samples of the random terpolymer (▲, dashed-line) and the block copolymer (●, full line) as a function of the isothermal crystallisation temperature.

layer. We have compared the intensity distribution along each of these layer lines which the equivalent functions calculated for the α crystal structure, for example Fig. 8 in Ref. [14]. There is excellent correspondence between observed and calculated values confirming the presence of the α phase.

Fig. 7(b) shows the map of the scattered X-ray intensity for fibres of the random terpolymer which have been hot drawn at 40 °C to an extension ratio of 8 and then annealed at 80 °C. The equatorial section contains three peaks at $|Q| \sim 1.16$, 1.52, and 2.00 $Å^{-1}$ and peaks at $|Q| \sim 1.20$ and 2.14 $Å^{-1}$ in the meridional section. The pattern has many features in common with that for the poly(L-lactide) although there is clearly a much larger non-crystalline component as can be seen from the diffuse isotropic scattering centred on $|Q| \sim 1.2$ $Å^{-1}$. Although the structure

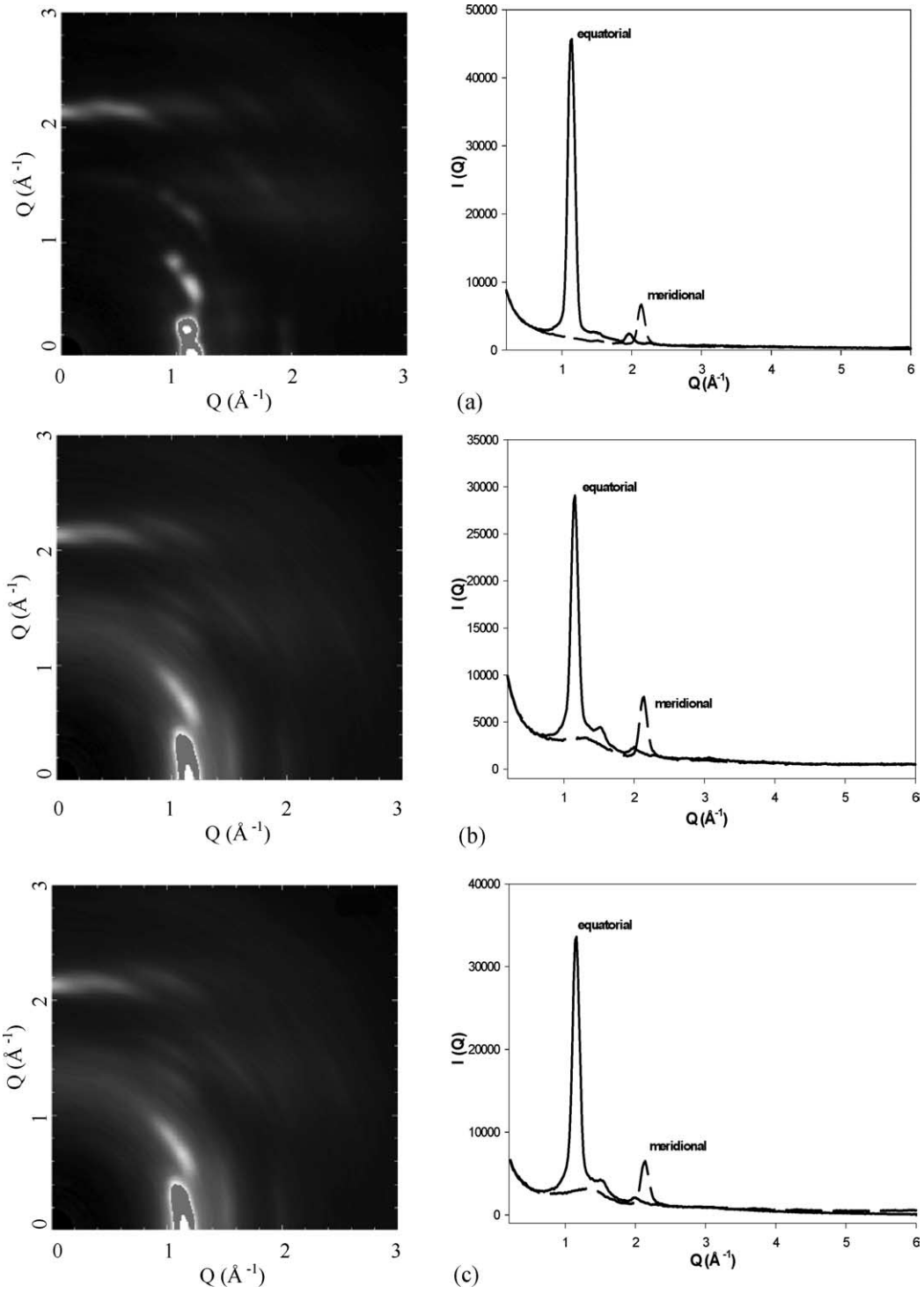

Fig. 7. X-ray scattering intensity maps $I(Q,\alpha)$ for the annealed fibres of (a) poly(L-lactide), (b) random terpolymer and (c) block terpolymer. In each case the fibre axis is vertical. The grey scale representation is arranged to that white represents the highest intensity. Note that the grey scale has been truncated to allow the details within the pattern to be observed. The relative strength of the strong equatorial feature at $|Q| \sim 1.2$ Å^{-1} can be judged from the equatorial section. The accompanying line plots show the equatorial ($\alpha = 0°$, full line) and the meridional section ($\alpha = 90°$, broken line).

is somewhat smeared, probably as a result of somewhat smaller crystals, it is clear that the pattern of intensity of the sharper crystalline features observed for the poly(L-lactide) are reproduced in the random terpolymer pattern. The positions of the *hk*0 reflections, the layer line spacing and the distribution of intensity along each layer line (Fig. 8(b)) are more or less equivalent between homopolymer and random terpolymer although the sparcity of higher order *hk*0 reflections makes calculation of the unit cell for the latter rather

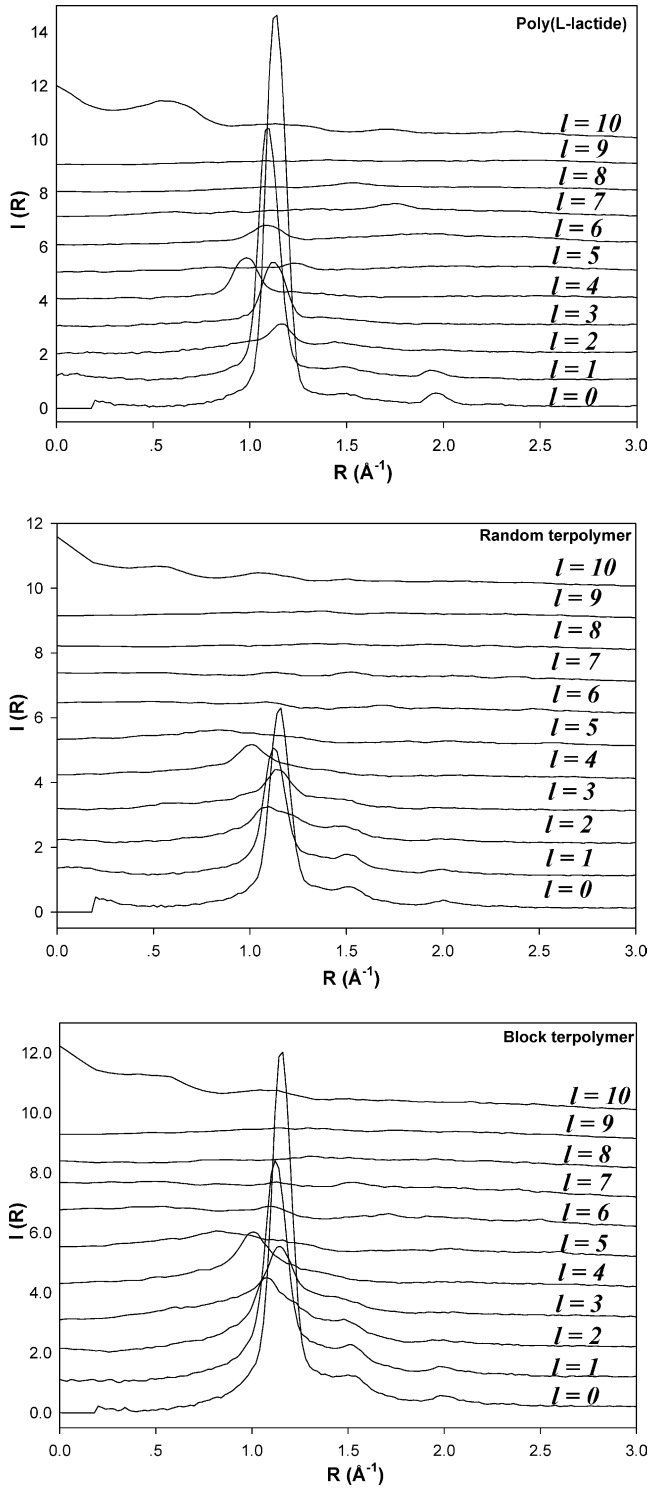

Fig. 8. Cross sections of the intensity maps shown in Fig. 7 taken at constant Z values corresponding to the layer line number indicated in the figures.

imprecise. However, it is clear that the crystal structure is equivalent to the α phase of poly(L-lactide).

A similar pattern of observations can be made with respect to the intensity map for the block copolymer (Fig. 7(c)). The block copolymer exhibits three peaks at $|Q| \sim 1.16$, 1.52 and 1.98 on the equatorial section and two peaks ~ 1.30 and 2.14 Å^{-1} on the meridional axis. Again a comparison of the features including the layer line intensity distributions (Fig. 8) confirms the presence of a crystal structure equivalent to the α phase of poly(L-lactide). The strong equatorial feature at $|Q| \sim 1.2$ Å^{-1} which corresponds to the 110 peak in the α phase and is present in all three fibre patterns has a breadth at half height of ~ 0.15 Å^{-1}. A similar breadth is observed for the 0, 0, 10 reflection on the meridian. This corresponds to crystal sizes of the order of 50 Å, although we have not corrected for any instrumental broadening.

For the α phase of poly(L-lactide), meridional reflections should be limited to the 10th, 20th etc layer lines. A number of authors have reported the presence of meridional reflections on other layer lines which they have interpreted as arising from non-integer helices and variation in the up-down symmetry of neighbouring chains [9–11,14]. For the poly(L-lactide) annealed fibre we observed some very weak scattering on the 7th layer line on the meridional axis. However, as with Sasaki et al. [14] we have attributed this to streaking from nearby reflections on the same layer line. Other than a very weak reflection at ~ 4.30 Å^{-1} corresponding to the 20th layer line, we did not observe meridional reflections on any other layer lines.

The small-angle X-ray scattering pattern for the as-spun filaments of the random or block terpolymer shows no distinctive features other than a small level of continuous scattering from simple density fluctuations. This suggests that the block copolymer does not exhibit any microphase segregation in the melt. This is not surprising as there will be quite a broad distribution of the block lengths from one polymer chain to another. In contrast, the patterns recorded for the annealed fibres show very strong and highly anisotropic scattering features as shown in Fig. 9. For the random copolymer (Fig. 9(a)) we see very sharp meridional peaks indicating a highly aligned two phase structure. The azimuthual variation of intensity is probably defined by the resolution of the instrument rather than any slight misorientation of the crystallites. The peak position is 0.038 Å^{-1} and the peak width is 0.01 Å^{-1}. There is also an equatorial streak which probably arises from micro voids in the original as-spun fibre which have been extended during hot drawing. The block copolymer fibre shows a similar pattern but the scattering is very much weaker with maxima at 0.031 Å^{-1} and a peak width of 0.02 Å^{-1}.

The WAXS and SAXS data provides a detailed view of the multiple phase morphology. For both terpolymers the crystallites are formed from the lactide units. There is no evidence for any crystal structure corresponding to that exhibited by poly(caprolactone) [35]. The lactide units crystallise in a structure equivalent to the α phase of poly (L-lactide). The block terpolymer crystallises more rapidly presumably due to the greater mobility of the end blocks but the random terpolymer displays a highly developed lamellar stack type SAXS pattern, suggesting better defined crystals than in the block copolymer system where the equivalent

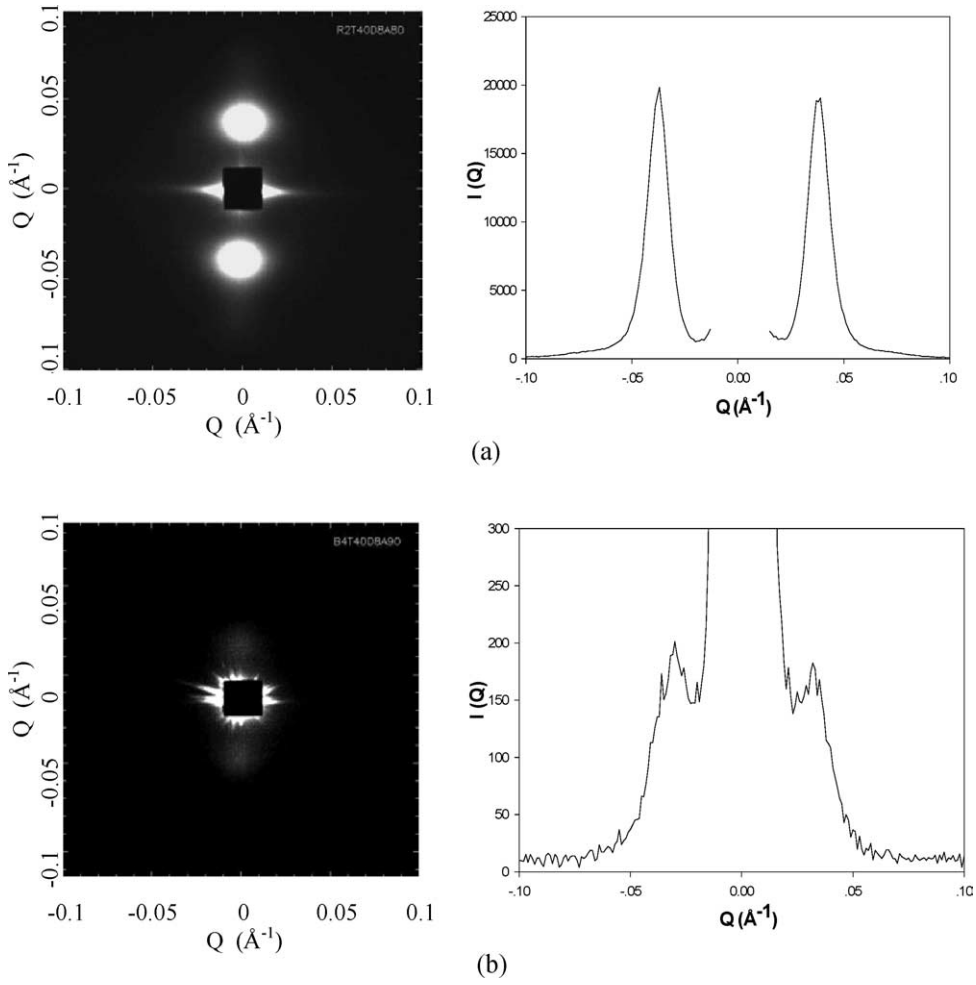

Fig. 9. Small-angle X-ray scattering patterns recorded for the same annealed fibres as in Fig. 7 i.e. (a) annealed random terpolymer and (b) annealed block copolymer. In each case the fibre axis is vertical. The dark square in the centre is the shadow of the beam stop. In Fig. 9(b), the scattering is much weaker than in Fig. 9(a) and some scattering from the collimation system can be seen around the beam stop in the form of short spikes.

SAXS is rather weak. The SAXS patterns give long periods of the order of 160 Å for the random terpolymer and 200 Å for the block terpolymer. With crystallinity levels as recorded in Fig. 6, this suggests crystal sizes of the order of 40 Å similar to those derived from the meridional peaks. The lactide sequence in either the random or terpolymer determined by NMR is of the order of 10 which corresponds to 60 Å for a chain in a 10/3 helix conformation.

7. Structure of un-annealed samples

Although the annealed fibre patterns are an excellent basis for structural analysis, such fibres are unsuitable for use as absorbable sutures as they are too stiff and exhibit a high level of crystallinity. In Fig. 10 we show the X-ray scattering patterns for the random and block terpolymers prepared under conditions (low draw ratio, low draw temperature, no annealing) which yield filaments more suited for use as absorbable sutures [2]. Comparison of these patterns with those for the annealed fibres (Fig. 7) reveals a greater extent of azimuthual arcing indicating a lower level of orientation. This serves to smear the features. We can identify an intense feature on the equatorial sections at $Q=1.16$ Å^{-1} and a rather weaker meridional feature at $Q=2.14$ Å^{-1} in the pattern for the random terpolymer. The block terpolymer pattern exhibits an intense equatorial feature at $Q=1.16$ Å^{-1} and a meridional feature at $Q=2.18$ Å^{-1}. The breadth of the equatorial peak for the block copolymer ($\Delta Q=0.34$ Å^{-1}) is about twice that observed for the equivalent peak in the pattern for the random terpolymer. The breadths of the meridional features are $\Delta Q=0.31$ Å^{-1} for the block terpolymer and $\Delta Q=0.25$ Å^{-1} for the random terpolymer.

Comparison of the fibre patterns with the equivalent patterns recorded for the annealed fibres suggests that the structures are similar but clearly we can not identify directly the well defined layer lines present in Fig. 8. Extracting structural information from fibre patterns with partial alignment is a long standing problem and a variety of techniques have been proposed. Most methods focus on procedures to deconvolute the observed pattern with the

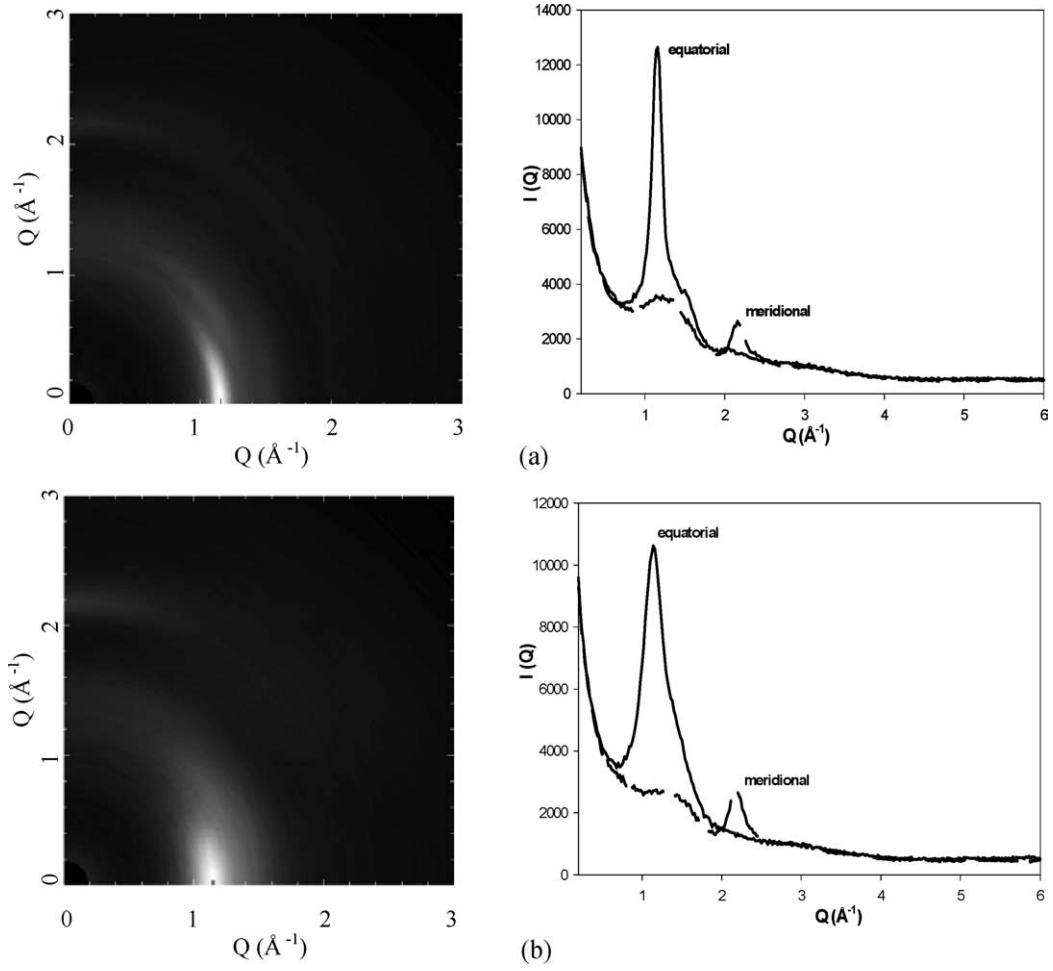

Fig. 10. X-ray scattering intensity maps $I(Q,\alpha)$ for the unannealed fibres of (a) random terpolymer and (b) block terpolymer. In each case the fibre axis is vertical. The grey scale representation is arranged to that white represents the highest intensity. Note that the grey scale has been truncated to allow the details within the pattern to be observed. The relative strength of the strong equatorial feature at $|Q| \sim 1.2$ Å^{-1} can be judged from the equatorial section. The accompanying line plots show the equatorial ($\alpha = 0°$, full line) and the meridional section ($\alpha = 90°$, broken line).

estimated orientation distribution. Such approaches usually run in to problems concerned with estimating the orientation distribution function and in the numerical processing. We have used a somewhat simpler but rather novel approach which is introduced below.

The scattering for a fibre sample exhibiting a partial level of preferred orientation, $I(|Q|,(\alpha)$, can be written as the convolution of the scattering for a perfectly aligned system $I^0(|Q|,(\alpha)$ with the orientation distribution function $D(\alpha)$:

$$I(|\underset{\sim}{Q}|, \alpha) = I^0(|\underset{\sim}{Q}|, \alpha) D(\alpha) \tag{2}$$

The function $D(\alpha)$ describes the distribution of the structural units with respect to the symmetry axis of the sample.

If we express the intensity functions and the orientation distribution function in terms of a series of spherical harmonics, $I_{2n}(|\underset{\sim}{Q}|)$, $I^0_{2n}(|\underset{\sim}{Q}|)$ and D_{2n} we can write this convolution as [36,37]:

$$I_{2n}(|\underset{\sim}{Q}|) = \left\{\frac{2\pi}{(4n+1)}\right\} D_{2n} I^0_{2n}(|\underset{\sim}{Q}|), \alpha) \tag{3}$$

where $n = 0, 1, 2, 3 \ldots \infty$. We only need the even terms of each series as the pattern will exhibit an inversion centre intrinsic to an X-ray scattering pattern for a non-absorbing fibre. The components of each series can be obtained by [37]:

$$I_{2n}(|\underset{\sim}{Q}|) = (4n+1) \int_0^{\pi/2} I(|\underset{\sim}{Q}|, \alpha) P_{2n}(\cos\alpha) \sin\alpha \, \mathrm{d}\alpha \tag{4}$$

and related expressions, where $P_{2n}(\cos\alpha)$ are a series of spherical harmonics [37], for example, $P_0 = 1$, $P_2(\cos\alpha) = (3\cos^2\alpha - 1)/2$. The complete scattering pattern may be recovered by:

$$I(|\underset{\sim}{Q}|, \alpha) = \sum_{2n=0}^{2n=\infty} I_{2n}(|\underset{\sim}{Q}|) P_{2n}(\cos\alpha) \tag{5}$$

The value of this representation is that the effects of preferred orientation are separated from the dependence of

the scattering on the spatial correlations [37,38]. Eq. (3) shows that for samples with the same structure, the variation of the amplitudes of the spherical harmonics $I_{2n}(|Q|)$ with $|Q|$ are essentially the same, with a simple constant multiplier dependent on the level of preferred orientation. The orthogonal nature of the spherical harmonics in Eq. (3) means that for multiple phase structures as considered here, where the scattering from the different phases is additive, the resultant spherical harmonics will also be linear combinations of the harmonic functions for each phase.

To check the efficacy of this approach, we have compared the first four components (Fig. 11) of the series of spherical harmonics derived from the patterns shown in Fig. 7, i.e. the annealed fibres. The weight of any feature in a harmonic is a function of the fraction of the material which exhibits that structure and the level of preferred orientation as well as the relative strength of the underlying structure factor.

We identified above, that the structure in each fibre contains an anisotropic structure which involves both crystalline and non-crystalline components and some isotropic scattering from a unoriented amorphous structure. The spherical harmonics for $2n>0$ represent the anisotropic scattering and hence they will contain only the crystalline and aligned non-crystalline scattering. If we compare the three curves each of Fig. 11(a)–(d) it is clear that each of the features (i.e. maxima and minima) observed in the appropriate spherical harmonic are reproduced in the equivalent functions derived from the scattering for the two terpolymers. The variations in height reflect the small differences in preferred orientation between the three fibre samples. The curves for $2n=0$ (Fig. 11(a)) show larger differences due to the variations in crystallinity between the three samples as reflected most clearly in the height of the sharp peak at $|Q|=1.18$ Å^{-1}. Despite such differences in weightings, we can discern that the various features present in the poly(L-lactide) sample are also present in the equivalent curves for the two terpolymer fibres. These observations underpin the observations already made above using the complete patterns and the layer line plots. Clearly the method is effective and does not require any assumption about the orientation distribution function or numerical approximations.

Fig. 12 shows the first four spherical harmonic

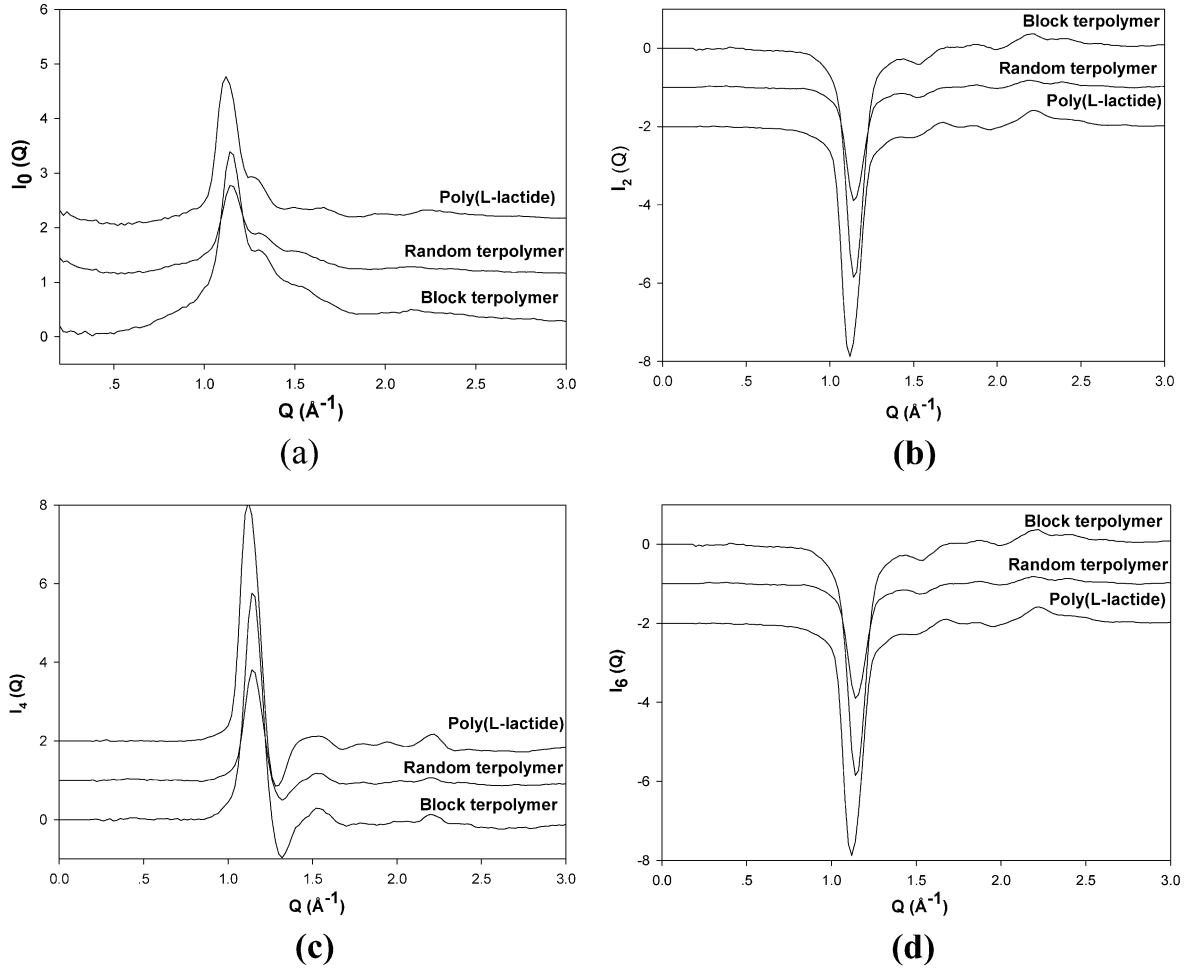

Fig. 11. A comparison of the amplitudes of the series of spherical harmonics which represent the fibre patterns shown in Fig. 7 for the annealed samples of the poly(L-lactide), the random and block terpolymers. Each curve has been offset for clarity but in all cases the value of the functions at $|Q|=0.0$ Å^{-1} is zero.

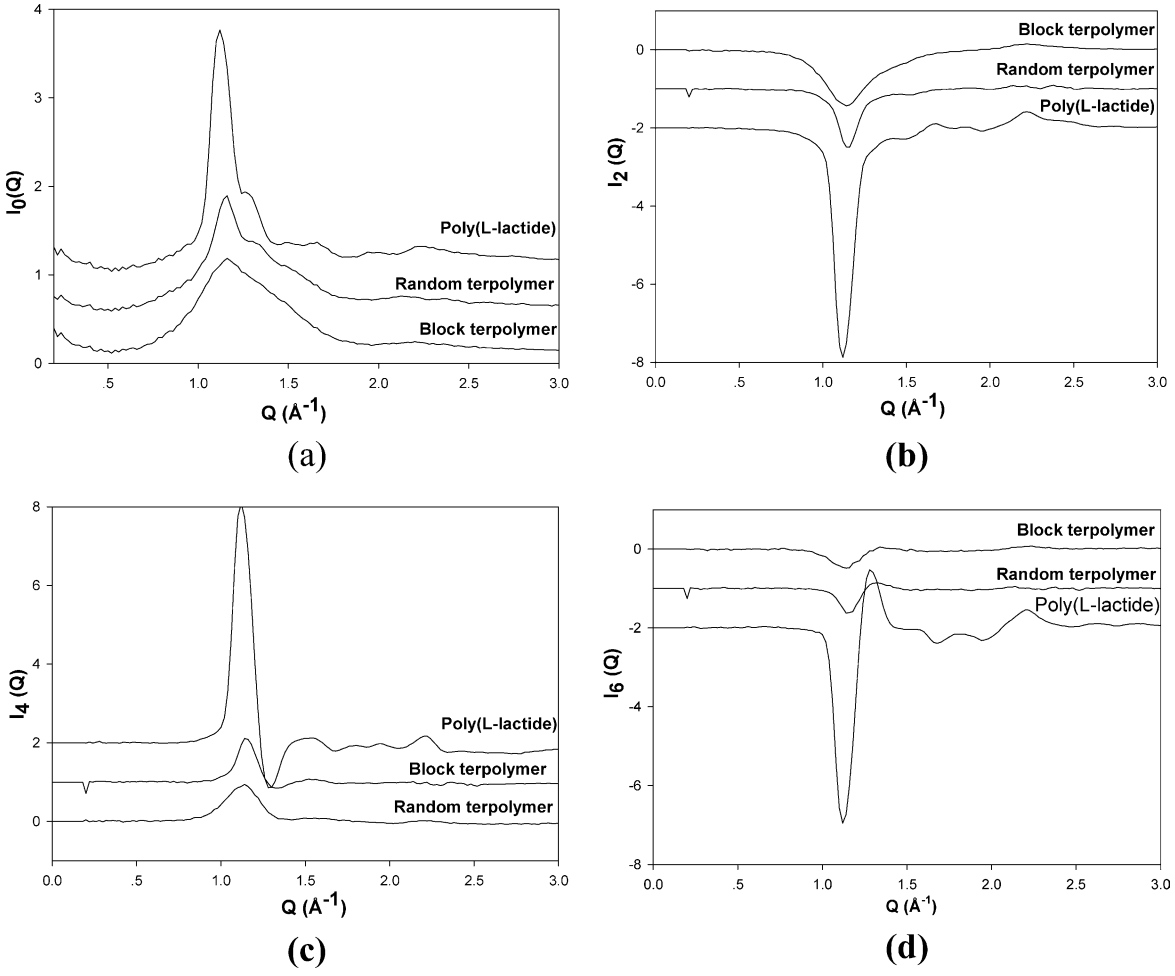

Fig. 12. A comparison of the amplitudes of the series of spherical harmonics which represent the fibre patterns shown in Fig. 10 for the unannealed samples of the random and block terpolymers with those derived from the annealed poly(L-lactide) shown in Fig. 7.

components derived from the scattering patterns shown in Fig. 10 compared to those derived from the scattering pattern of the poly(L-lactide) shown in Fig. 7(a). If we consider the curves for $2n>0$ it is clear that the features for the poly(L-lactide) are very much more intense than those observed in the curves relevant to the terpolymer fibres. This simply reflects the higher proportion of anisotropic material and the higher level of preferred orientation present in the poly(L-lactide) fibre. In terms of the key minima and maxima ($|Q|=1.18$, 1.3 and 2.4 Å^{-1}), the curves are equivalent indicating that it is reasonable to conclude that the terpolymer filaments prepared at low draw ratios and without annealing exhibit a similar crystal structure to poly(L-lactide) despite the smaller crystal size and greater crystal misorientation.

8. Structure of un-drawn fibres

In order to confirm that the drawing does not induce any changes to the crystal structure other than the level of preferred orientation and degree of crystallinity, we have crystallised samples of the three polymers from quiescent melts and recorded the X-ray scattering intensity as a function of $|Q|$ using the same diffractometer as employed to record the fibre scattering data. The fully corrected and scaled intensity functions are shown in Fig. 13.

In order to compare the scattering from these isotropic samples with that from the fibres we have calculated the scattering expected for an isotropic sample with the same structure as the hot-drawn fibres. Experimentally, this would be achieved by powdering the fibre in to small parts which are then arranged randomly. It is more straightforward to perform the azimuthual averaging numerically using the scattering pattern for each fibre. The scattering pattern for a sample containing the same fibrous structure but with the fibre axis arranged at every angle possible with respect to the scattering vector is given by:

$$I_{\text{isotropic}}(Q) = \int_0^{\pi/2} I(Q,\alpha)\sin\alpha \mathrm{d}\alpha \tag{7}$$

Comparison of Eqs. (4) and (7) shows that $I_{\text{isotropic}}(Q)$ is equivalent to $I_0(Q)$ (as in Figs. 11 and 12) and these functions are also plotted in Fig. 13. We can see that the

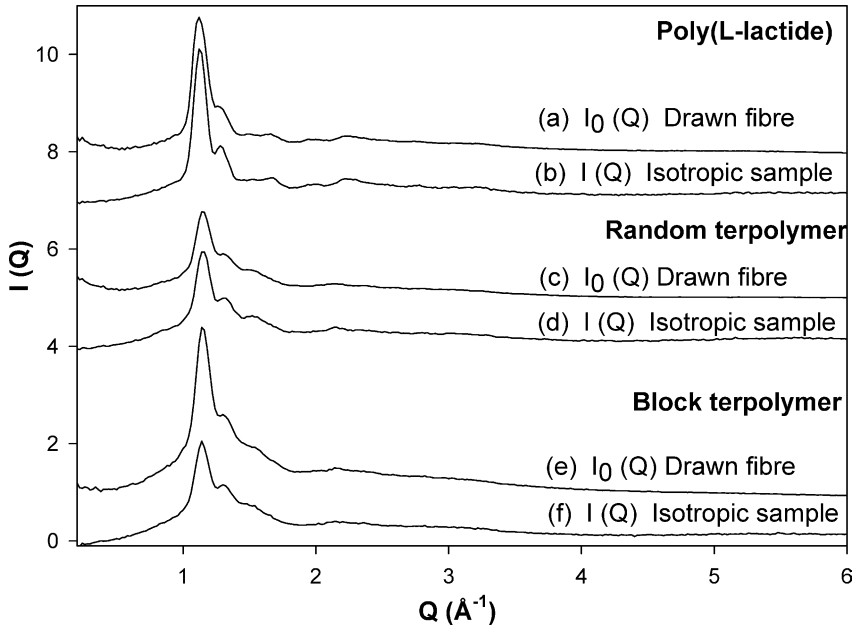

Fig. 13. Plots of the fully corrected and scaled wide-angle X-ray scattering intensity $I(Q)$ recorded for samples of poly(L-lactide) (PLLA), random terpolymer and block terpolymer crystallised from a quiescent melt compared to the azimuthually averaged data $I_0(Q)$ for each annealed fibre as described in the text. The azimthually averaged data represents a sample with no global preferred orientation but the same localised structure as the fibres.

curves are essentially the same in terms of peak positions and overall shapes. In the case of the block terpolymer, the height of the intense peak at $|Q| \sim 1.2$ Å^{-1} in the curve for the isotropic sample is somewhat smaller than derived from the fibre pattern showing that that hot-drawing and annealing has increased the level of crystallinity. This effect is very much less marked in the case of the random terpolymer and in poly(L-lactide).

9. Discussion

Fibre diffraction studies are conventionally performed on highly aligned fibres which have often been extensively treated to enhance the levels of crystallinity; the work of Sasaki et al. [14] is an example where the fibre has been treated to degrade the polymeric structure in order to enhance the crystallinity. In this work we have introduce a new tool in the study of fibres which allows the X-ray scattering patterns for structures with differing levels of preferred orientation to be compared directly with out recourse to arbitrary processes or the separation in to the scattering from phases. The method employs a representation of the data as a series of spherical harmonics. The methodology has been applied to two terpolymers with rather different architectures but both involving sequences of randomly distributed lactide units with sequence lengths of $\sim$10, although their positioning in the molecular chain differs. We have prepared highly drawn monofilaments which have shown that both systems exhibit a semi-crystalline structure in which the lactide units crystallise in a structure equivalent to the α phase of poly(L-lactide). Of course there are some limitations to this novel approach but the two annealed terpolymer fibres exhibit structures equivalent to the α phase of poly(L-lactide). The helical structure of the lactide sequences does not appear to be distorted as no systematically absent 00l type reflections were observed. This contrasts with studies of the poly (L-lactide) homopolymer [14] and may arise from the less specific chain interactions which may be present in the rather more disordered copolymer structures. These weaker interchain interactions make a specific regular chain conformation more likely.

A particular feature of this new approach, is that we can study the crystalline structure of fibres more relevant to application, for example with the biodegradable terpolymers studied here, use as absorbable sutures is promising application. In the low draw ratio terpolymer fibres, it is clear that despite the lower level of orientation and rather small crystal size ($\sim$20–30 Å) the crystal structure remains largely the same. Comparison of the annealed and unannealed fibre patterns and associated sections shows the significant effect of annealing on the apparent crystal size. This is more marked for the block copolymer system. Comparison of scattering obtained from samples prepared via a quiescent melt phase shows that the drawing process does not affect the crystal structure but it does influence the level of crystallinity most markedly in the block copolymer system. This system exhibits a maximum in the crystallisation rate for quiescent systems at a slightly higher temperature than that recorded for the random terpolymer. This can be related to the differences in T_m and T_g for the

two terpolymers, essentially the peak crystallisation rates occur at the same level of undercooling midway between T_m and T_g. We attribute the increased level of crystallinity in the case of the block terpolymer after drawing to the enhanced mobility of the end blocks in the block copolymer system. We did not see any evidence that there was micro phase segregation in the block terpolymer melt prior to hot drawing which might also influence the rate of crystallisation. However, it is clear that on the larger scale the two phase crystalline/non-crystalline structure is rather ill-defined in the block copolymer case. We attribute this to the range of block lengths present in the polymer chains and the rather disrupting (i.e. non-inclusion) effect of the highly disordered central block containing very short sequences of both lactide and caprolactone. In contrast, the random copolymer exhibits a rather well defined two-phase structure which we attribute to the greater extent that non-lactide units can be incorporated in to the interfaces of lamellar crystals to provide a smoother crystal face. This variation in the structure and dynamics of two materials with similar chemical composition but rather different architectures will be most helpful in the optimisation of these materials for use in biomedical applications.

10. Summary

Random or block terpolymers containing ~70 mol% of lactide units with a balance of caprolactone and glycolide moieties exhibit a semi-crystalline structure in which the crystal component is essentially equivalent to the α crystal phase of poly(L-lactide). The crystal structure appears to be largely invariant to different processing conditions for as to whether the terpolymer is crystallised under quiescent conditions or hot-drawn from pre-spun filaments to low or high draw ratio. This contrasts with the behaviour of the poly(L-lactide) homopolymer which exhibits a number of crystal forms, although the fibres prepared in this work under similar conditions to those used for the terpolymers also generates the α form. The level of crystallinity is enhanced in the block terpolymer samples which are subjected to hot drawing but this is not the case for the random copolymer. In contrast, the random copolymer appears to have a very much better defined lamellar structure which we attribute to the ability of the random copolymer to incorporate minor levels of the other units in to the crystal interface in order to achieve a smoother crystal surface. The use of the spherical harmonic representation of the fibre patterns considerable facilitates comparison between the annealed and unannealed fibres and samples crystallised from quiescent melts. This is particularly important for understanding the chemistry-structure-property relationships in these complex disordered polymer monofilaments with potential for use as absorbable sutures.

Acknowledgements

This work was supported by the National Metal and Materials Technology Centre (MTEC), Thailand and the Royal Society, UK, through the award of South-East Asia Fellowship to JS. The small-angle X-ray scattering data were obtained using beam-line 16.1 at the CCLRC Daresbury synchrotron radiation source and we thank the beam-line scientist Anthony Gleeson for his help with the SR experiments. We thank the Thai Ministry of University Affairs and the Graduate School, Chiang Mai University for financial support.

References

[1] Bezwada RS, Jamiolkowski DD, Lee IY, Agarwal V, Persivale J, Trenkabenthin S, et al. Biomaterials 1995;16:1141–8.
[2] Buntner B, Nowak M, Kasperczyk J, Ryba M, Grieb P, Walski M, et al. J Control Release 1998;56:159–67.
[3] Cai Q, Bei JZ, Wang SG. Polym Adv Technol 2002;13:105–11.
[4] Cai Q, Bei JZ, Wang SG. Polymer (B) 2002;43:3585–91.
[5] Dawes E, Rushton N. Biomaterials 1997;18(24):1615–23.
[6] Cordewener FW, Dijkgraaf LC, Ong JL, Agrawal CM, Zardeneta G, Milam SB, et al. J Biomed Mater Res 2000;50:59–66.
[7] Hasirci V, Lewandrowski KU, Bondre SP, Gresser JD, Trantolo DJ, Wise DL. Bio-Med Mater Eng 2000;10:19–29.
[8] Honda M, Yada T, et al. J Oral Maxillofacial Surgery 2000;58(7): 767–75.
[9] De Santis P, Kovacs J. Biopolymers 1968;6:299–306.
[10] Hoogsteen W, Postema AR, Pennings AJ, ten Brinke G, Zugenmaier P. Macromolecules 1990;23:634–42.
[11] Kobayashi J, Asahi T, Ichiki M, Oikawa A, Suzuki H, Watanabe T, et al. J Appl Phys 1995;77:2957–73.
[12] Cartier L, Okihara T, Ikada Y, Tsuji H, Puiggali J, Lotz B. Polymer 2000;21:8909–19.
[13] Puiggali J, Ikada Y, Tsuji H, Cartier L, Okihara T, Lotz B. Polymer 2000;21:8921–30.
[14] Sasaki A, Asakura T. Macromolecules 2003;36:8385–90.
[15] Cai Q, Bei JZ, Wang SG. Acta Polym Sin 1999;761–4.
[16] Srisa-ard M, Molloy R, Molloy N, Siripitayananon J, Sriyai M. Polym Int 2001;50:891–6.
[17] Cai Q, Bei JZ, Wang SG. Polym Adv Technol 2000;11:159–66.
[18] Nijenhuis AJ, Grijpma DW, Pennings AJ. Macromolecules 1992;25: 6419–24.
[19] Flory PJ. J Chem Phys 1947;15:684.
[20] Flory PJ. J Chem Phys 1949;17:223.
[21] Windle AH, Viney C, Golombok R, Donald AM, Mitchell GR. Faraday Discuss 1985;79:55.
[22] Dobrzynski P. J Polym Sci, Part A: Polym Chem 2002;40:3129–43.
[23] Kasperczyk J, Bero M. Makromol Chem 1991;192:1777–87.
[24] Bero MJ, Kasperczyk J, Adamus G. Makromol Chem 1993;194: 907–12.
[25] Kasperczyk J, Bero M. Makromol Chem 1991;194:913–25.
[26] Kasperczyk J, Bero M. Makromol Chem 1993;194:913–25.
[27] Mitchell GR. In: Allen G, Bevington J, editors. Comprehensive polymer science, vol. 1. New York: Pergamon Press; 1989. p. 687–729 [chapter 31].
[28] Bassett D. J Macromol Sci Phy 2003;B42:227.
[29] Sarasua JR, Prud'homme RE, Wisniewski M, Le Borgne A, Spassky N. Macromolecules 1998;31:3895–905.
[30] Vasanthakumari R, Penning JA. Polymer 1983;24:175–8.
[31] Tsuji H, Ikada Y. Polymer 1995;36:2709–16.

[32] Walsh DR. In: Booth C, Price C, editors. Comprehensive polymer science, vol. 2. New York: Pergamon Press; 1989. p. 135 [chapter 5].
[33] Perrin DE, English J. In: Domb AJ, Kost J, Wiseman DM, editors. Handbook of biodegradable polymers. New York: Harwood Academic Publishers; 1997. p. 3 [chapters 1 and 3].
[34] Fischer EW, Serzel HJ, Wegner G. Kolloid Z Polym 1973;251:980.
[35] Chatani Y, Okita Y, Tadokoro H, Yamashita Y. Polym J 1970;1: 555–62.
[36] Lovell R, Mitchell GR. Acta Cryst 1981;A37:135.
[37] Mitchell GR, Windle AH. Colloid Polym Sci 1982;260:754.
[38] Mitchell GR, Saengsuwan S, Bualek-Limcharoen S. Prog Colloid Polym Sci 2005;130.